Reaction Kinetics, Mechanisms and Catalysis (2023) 136:1737–1755
https://doi.org/10.1007/s11144-023-02402-2

A sustainable approach for the removal of toxic 4-nitrophenol in the presence of H_2O_2 using visible light active Bi_2MoO_6 nanomaterial synthesized via continuous flow method

Brijesh Kumar Shukla[1] · Mayank Kumar Gautam[2] · Shalu Rawat[2] · Hema Bhandari[3] · Jiwan Singh[2] · Seema Garg[1]

Received: 14 February 2023 / Accepted: 27 March 2023 / Published online: 3 April 2023

Abstract

In the present study, a visible-light active nanosized Bi_2MoO_6 was prepared by a continuous flow method. The synthesized nanomaterials were characterized by powder X-ray diffraction (PXRD), scanning electron microscope (SEM) coupled with energy dispersive spectroscopy (EDS), UV–visible analysis, Fourier transform infrared spectroscopy (FTIR), and zero-point charge (pH_{ZPC}). The band gap energy of the photocatalyst was found to be 2.81 eV, which shows it is a visible light active material. The prepared catalyst was applied for the photocatalytic degradation of a harmful organic pollutant, 4-Nitrophenol (4-NP), under the irradiation of visible light, and its photodegradation was enhanced by hydrogen peroxide. Furthermore, photo-degradation efficiency was optimized by a statistical method, considering critical process parameters such as concentration of 4-NP, pH, temperature, catalyst loading, and time. The maximum photocatalytic activity was achieved when experimental parameters such as pH were maintained at about 7.0 and catalyst dosage, H_2O_2 concentration, and 4-NP concentration were 1 g/L, 0.025 mol/L, and 10 mg/L, respectively, at 35 °C. The maximum photodegradation was 93% and it was majorly governed by the participation of the $OH^{\cdot}$ radical. The pseudo-first order reaction kinetics was evaluated and fitted for the degradation of 4-NP. Furthermore, a possible mechanism based on the generation of electron holes for 4-NP degradation has also been proposed in the present work. This method is found to be efficient, environmentally friendly, and free of toxic materials.

Keywords Bismuth molybdate · Photocatalysis · 4-NP · Degradation · Statistical analysis

✉ Seema Garg
sgarg2@amity.edu

Extended author information available on the last page of the article

Introduction

In the past few years, our water resources have been contaminated to a greater extent due to discharges of untreated effluents from different industries. A large number of organic pollutants are released by these effluents, which threaten the supply of potable water. 4-NP is among the most abundantly found organic pollutants in water as it is utilized in numerous intermediate industrial processes [1]. 4-NP is a benzene derivative and is formed by the connection of hydroxyl and nitro groups with the benzene ring, which is called para-nitrophenol. These compounds are used in dyes, drugs, pesticides, polymers, plasticizers, and explosives [2], and they are highly toxic and carcinogenic in nature. The permissible limit of such benzene derivatives in potable water is determined to be 0.5 ppb and 0.5 to 1.0 ppm in wastewater discharge [3]. A higher tendency of 4-NP to make derivatives leads to the formation of compounds like 4-chloronitrophenol, which is even more toxic and biodegradation resistant [4]. 4-NP is a basic key raw material for nitroaromatic derivatives and is used in the commercial production of paracetamol, also called acetaminophen, and in the production of pesticides such as methyl-parathion and parathion [5]. In the water discharge, these pesticides are also considered to be a major source of 4-NP detected in the environment since they can be converted to 4-NP under the action of hydrolase [6]. 4-NP is considered a persistent toxic pollutant [7, 8] and its toxicology and carcinogenicity have been studied [9, 10], and the acute toxicity of 4-NP leads to blood disorders, chromosomal abnormalities, feeling sleepy, and cyanosis [11, 12].

As a result, 4-NP is listed as a priority pollutant by regulatory bodies. Hence, removal of 4-NP from wastewater is an urgent need before being discharged into the environment. In the same direction, numerous methods have been reported by researchers for 4-NP degradation viz., bio-degradation [13], advance oxidation process (AOP) [14, 15], chemical redox [16, 17], heterogeneous photo-catalysis [18, 19], adsorption techniques [20], sonolysis [21] and Fenton chemistry [16, 22].

Due to their electronic structure, metal oxide semiconductors such as ferric oxide (Fe_2O_3), titanium oxide (TiO_2), zinc oxide (ZnO), oxides of bismuth such as BiOBr, $BiVO_4$, $BiWO_6$, Bi_2O_3, sulphide of cadmium sulphide (CdS), zinc sulphide (ZnS), $Sr_2Nb_2O_7$, and Bi_2MoO_6 can act as sensitizers for light-reduced redox reactions [23, 24, 25]. Due to its potential for degrading organic and inorganic contaminants through a process known as heterogeneous photocatalysis, semiconductor- based photocatalysis has attracted a great deal of interest in recent times [26]. It is based on the generation of electron–hole pairs when a semiconductor is photo-illuminated with energy more than its energy gap. The reactive radicals produced by the charged species as they migrate to the semiconductor's surface begin redox reactions with the organics [27]. Heterogenous photocatalysis has been proven to be an efficient treatment method for the detoxification of phenolic substances. These semiconductor photocatalysts transform photon energy into chemical energy, and they have a lot of potential in the treatment of wastewater because they totally eliminate the contaminant rather than converting it into

another phase [28]. TiO_2 and bismuth molybdate have been the most considered photocatalysts in recent past due to their unique potential for water decontamination [29, 30].

The visible region accounts for the majority of solar light that reaches the earth's surface, but band gap of TiO_2 3.2 eV makes it unsuitable for use in this region of sunlight. Hence, efforts have been made to develop an alternative to TiO_2 and Bismuth molybdates, among which is being determined to have excellent efficiency in solar light mediated systems and has been shown to be capable of water splitting and environmental sanitization [31]. Oxides of bismuth have high oxide ion conductivity and electrocatalytic activity to inter-convert molecular and ionic oxygen at low temperatures; hence, they are found to be potentially important for the generation of oxygen [32]. A smaller band gap of 2.5–2.8 eV is responsible for its activity under visible light (420–500 nm) to degrade organic pollutants and the splitting of water [33, 34]. The fast and shortest synthesis of Bi_2MoO_6 (koechlinite) and $Bi_2Mo_3O_{12}$ nanoparticles in a continuous hydrothermal flow synthesis method was reported earlier [35], and a similar approach has been applied for the synthesis of nanosized Bi_2MoO_6 and synthesis of bismuth molybdate, which is done by a continuous flow method in a custom-designed tubular flow reactor and has a higher capability for large-scale production.

In the present study, the synthesis of visible light active nanosized bismuth molybdate photocatalyst was conducted using a continuous flow method, which makes it preferable for use in organic pollutants' decontamination under the illumination of solar light at low cost. The evaluation of the synthesized material has been carried out for the photocatalytic mineralization of 4-NP under the irradiation of visible light. Moreover, factors affecting the efficiency of degradation of 4-NP have also been studied, and the best-optimized condition has been explored for maximum degradation with the best-fitted model and factor range. The catalyst Bi_2MoO_6 was found to be more efficient and effective for the mineralization of very toxic 4-NP in aqueous solution.

Material and methods

Materials

All the raw materials used in the present work were of AR grade and were used without any further purification. The chemicals such as bismuth nitrate ($Bi(NO_3)_3{\cdot}5H_2O$), ammonium molybdate ($(NH_4)_6Mo_7O_{24}{\cdot}4H_2O$), Nitric acid ($HNO_3$), hydrochloric acid (HCl), sodium hydroxide (NaOH), 4-NP ($C_6H_5NO_3H$) and hydrogen peroxide (H_2O_2) used for the synthesis of photocatalyst were procured from Thermo Fisher Scientific.

Synthesis of nanosized Bi_2MoO_6 photocatalyst

Synthesis of the catalyst was done as per our previously reported continuous flow method [36] with minor modification. Aqueous solutions of bismuth precursor (0.2 mol $Bi(NO_3)_3{\cdot}5H_2O$ in 200 ml of 2 M nitric acid) (via pump 1) and an aqueous solution of molybdate precursor (0.2 mol $(NH_4)_6Mo_7O_{24}{\cdot}4H_2O$) in 400 ml of 2 M

aqueous NaOH) (via pump 2) were pumped with T mixture fed in preheated (at 210 °C, Zone-1, and pressure of 6–10 bar) in a custom-designed coil flow reactor and pH was maintained ~ 5–6. The process produces particle continuous flow to the cooling zone (at 50 °C, Zone-2, and pressure 6–10 bar) and the obtained slurry is continuously collected in a beaker from the exit of the back-pressure regulator. The collected slurry was centrifuged and the separated particles were washed with water and followed by ethanol, further dried in a hot air oven, and ground into a fine powder for further use.

Characterization

The SEM analysis was carried out by JSM 4490 JEOL, Japan, equipped with EDS. FTIR (NICOLET 6700) made by Thermo Fisher Scientific, U.S.A. was used to analyse the presence of functional groups on the surface of materials. The crystalline nature of the catalyst was analysed by XRD using D8 Advance Eco (Bruker, Germany), and the pH_{ZPC} of the catalyst was determined by the pH drift method as described in previous literature [37]. The UV–visible spectrum scanning was done using a UV–visible spectrophotometer (117 Systronics, India Limited).

Photocatalytic degradation

The photocatalytic degradation experiments were carried out in a 250 mL beaker inside a wooden chamber. A tungsten lamp was used as the source of visible light, with a radiation of 500 Lux on the surface of the reaction mixture. For degradation experiments, a 100 mL volume of 10 mg/L 4-NP was taken in the beaker and a determined amount of catalyst and H_2O_2 were added to it. It was stirred on the magnetic stirrer at 100 RPM inside the wooden chamber. The shaking was performed first in the dark for 30 min to check the amount of 4-NP removed by adsorption and then in the irradiation of visible light for 120 min. A 3 mL aliquot was withdrawn at different time intervals from the reaction mixture to determine the remaining concentration of the 4-NP after separation of the catalyst by centrifugation. The concentration of the 4-NP was analysed using a UV–Visible spectrophotometer at 317 nm. The percentage degradation was calculated as shown below in Eq. 1:

$$\%Degradation = \frac{C_0 - C_t}{C_0} \times 100 \tag{1}$$

Here, C_0 and C_t represents the concentration of 4-NP initially and after degradation, respectively. The degradation process was optimized by varying different operating conditions like catalyst concentration, H_2O_2 concentration, pH, initial pollutant concentration, reaction time, and temperature.

Results and discussion

Characterization of the catalyst

The morphological features of the synthesized Bi_2MoO_6 were analyzed by SEM, which are shown in Fig. 1a. The particles appear as aggregates with irregular shapes, and the size of some separate particles is less than 100 nm. The SEM analysis of the Bi_2MoO_6 after its application in the photocatalytic degradation process is shown in Fig. 1b, which also shows particles with irregular shapes. However, most of the particles after photocatalysis were observed to be of similar size, unlike before photocatalysis. The EDS analysis shows that the elemental composition of the catalyst was Bi, Mo, and O (Fig. 1c). The weight percentage of the elements is shown in Fig. 1c.

The UV–Visible analysis of the Bi_2MoO_6 was done in the range of 350 to 550 nm and the results are represented in Fig. 1d. The catalyst absorbed the spectrum in the visible range, which means that the catalyst is visible light active.

The steep shape spectra suggest absorption occurred due to a band gap transition [38]. The binding energy of the Bi_2MoO_6 was calculated from the Tauc's plot, which is represented in inset Fig. 1d. It was calculated to be 2.81 less than the conventionally used photocatalyst TiO_2 [39].

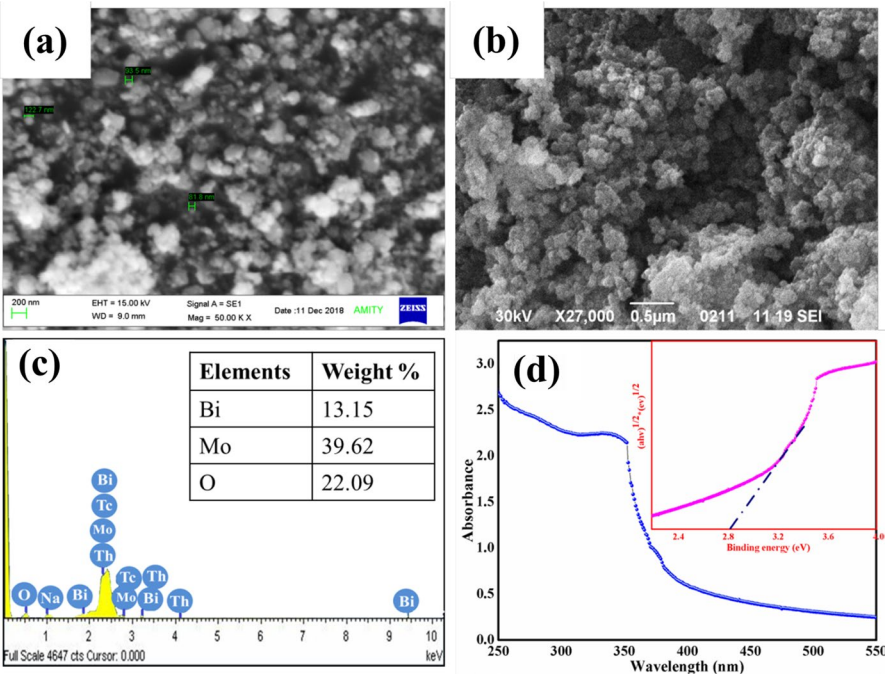

Fig. 1 **a** and **b** SEM analysis of Bi_2MoO_6 before and after photocatalysis, **c** EDS analysis and **d** UV–visible analysis (with Tauc's plot inset) of Bi_2MoO_6

The XRD analysis shows sharp peaks, which correspond to the crystalline nature of the catalyst (Fig. 2a). The peaks observed at $2\theta = 28.5°$ are attributed to the characteristic peak of Bi_2MoO_6 representing crystal plane 131 [40, 41]. Other peaks which were observed at positions $2\theta = 11.5°$, 23.69°, 33.3°, 36.0°, 38.6°, 39.91°, 46.7°, 47.33°, 55.5° and 58.4° corresponding to (060), (131), (222), (151), (400), (240)/(042), (202), (202), (331)/(133) and (262) planes of Bi_2MoO_6 (JC-PDS file 21-0102) [42, 43, 44, 45, 46]. The XRD pattern also shows minor impurities of bismuth and molybdate oxides, peaks presents at $2\theta = 25.8°$, 27.4° attributed to γ-Bi_2O_3 [47, 48] and peak at $2\theta = 49.06°$ is attributed to MoO_3 [49]. Results of FTIR analysis of Bi_2MoO_6 before and after photocatalysis of 4-NP are depicted in Fig. 2b. The spectrum was scanned in the range of 4000 to 400 cm^{-1} and shows a major peak at 3390 cm^{-1}, which corresponds to the vibrations in –OH bonds. This bond on the surface may appear due to the formation of hydroxides on exposure to the ambient environment or adsorption of water molecules. The peaks observed at wavelengths of 738 and 830 cm^{-1} correspond to the stretching of the Mo–O bond, asymmetric and symmetric, respectively, [50]. And a peak near 530 cm^{-1} represents the stretch in the Bi–O and Bi–O–Bi bonds [51]. The FTIR analysis of Bi_2MoO_6 after photocatalysis shows similar peaks, but the intensity of the peaks has changed. A new peak at ~ 3000 cm^{-1} appeared after photocatalysis corresponding to the C–H stretch [52]. The appearance of new peaks and changes in peak intensities may be caused by surface bond deformation caused by the adsorption of pollutants and degradation

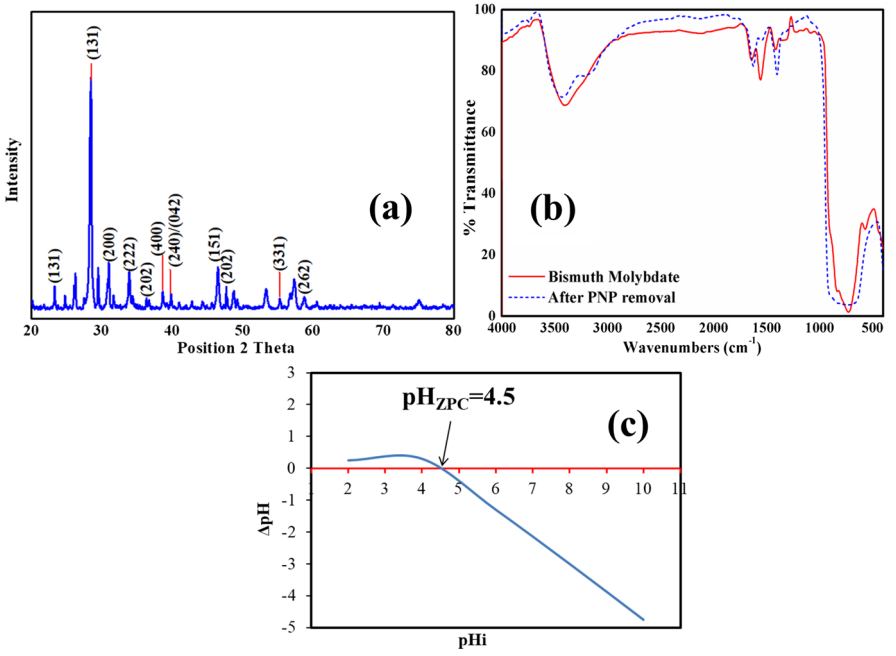

Fig. 2 **a** XRD analysis, **b** FTIR analysis and **c** pH_{ZPC} analysis of Bi_2MoO_6

products molecules on the catalyst's surface. The plot for pH_{ZPC} is shown in Fig. 2c, and the value of pH_{ZPC} was found to be 4.5.

Photocatalytic degradation of 4-NP

Control experiments

Prior to degradation experiments, six control experiments were run to confirm photocatalytic degradation of 10 mg/L 4-NP for 4 h at pH 7 and temperature 25 °C. Control 1 and 2 were run with Bi_2MoO_6 (BM) only under dark and under visible light irradiation (UVI). Controls 3 and 4 were run with H_2O_2 only, under the dark and under UVI, and controls 5 and 6 were run using BM in combination with H_2O_2 under the dark and under UVI. Results are expressed in Fig. 3a, control 1, 3, 4, and 5 showed a removal % of 4-NP < 10%. Maximum removal % was found in control 6 which was run with BM + H_2O_2 under UVI (93.8 ± 0.10) followed by control 2 (34.66 ± 0.26) which was run under UVI using BM only. The result shows that the effective removal of 4-NP was achieved under UVI using BM + H_2O_2 and BM only,

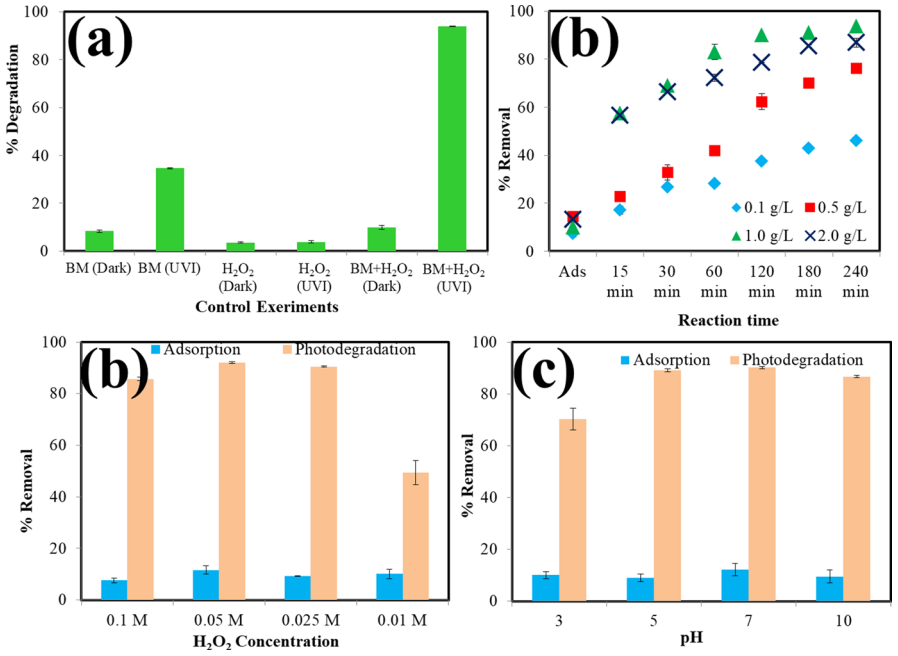

Fig. 3 **a** Control experiments (C_0 = 10 mg/L, Photocatalyst = 1 g/L, H_2O_2 concentration = 0.025 M, pH 7, Temperature = 25 °C), **b** Effect of photocatalyst amount (C_0 = 10 mg/L, H_2O_2 concentration = 0.025 M, pH 7, Temperature = 25 °C), **c** effect of H_2O_2 concentration (Photocatalyst = 1 g/L, C_0 = 10 mg/L, pH 7, Temperature = 25 °C) and **d** effect of pH (Photocatalyst = 1 g/L, C_0 = 10 mg/L, H_2O_2 concentration = 0.05 M, Temperature = 25 °C)

representing that the removal of 4-NP was resulted by photocatalytic degradation by BM under UVI only and the degradation % was enhanced by the addition of H_2O_2.

Effect of photocatalyst concentration

The effect of photocatalyst concentration on the degradation of 4-NP was studied in the range of 1.0 g/L to 2.0 g/L with a 10 mg/L initial concentration of 4-NP at pH 7. Fig. 3a shows that the degradation of the 4-NP was increased with increasing the concentration of photocatalyst from 1.0 to 2.0 g/L due to an increase in active sites for the generation of reactive species [53]. Similarly, Fahoul et al. [54] also observed an increase in photocatalytic degradation of acid red 1 by increasing the concentration of photocatalyst from 0.5 to 1.5 g/L due to an increase in active sites. However, a further increase in catalyst concentration up to 2.0 g/L resulted in less degradation. A lesser degradation percentage on further increasing the catalyst concentration may result due to the agglomeration of the catalyst particles due to which active sites overlap and less reactive species are generated. It may also occur due to the increase in opacity of the solution, which reduces the penetration of photons to the catalyst [55, 56, 57]. For the rest of the study, a 1.0 g/L concentration of catalyst was used.

Effect of H_2O_2 concentration

H_2O_2 acts as an electron acceptor, increasing the generation of reactive species ($OH^{\cdot}$) in the photocatalytic system. The concentration of H_2O_2 below or above the optimum concentration negatively affects the degradation process. The lower concentration of H_2O_2 generates an insufficient number of $OH^{\cdot}$ radicals, while the higher concentration of H_2O_2 generates an excessive number of $OH^{\cdot}$ radicals, which get destroyed by their collision with each other or H_2O_2 molecules [58, 59]. Therefore, the optimization of H_2O_2 concentration is required. In the present work, the effect of H_2O_2 concentration was studied in the range of 0.01 to 0.1 M (Fig. 3b), with an initial 4-NP concentration of 10 mg/L and pH 7. Hence, 0.05 M H_2O_2 was found to be optimum for the degradation of 4-NP and it was selected for further experiments.

Effect of pH

Operating pH is also an important factor in the catalytic degradation process it influences the charge on catalyst surface and degree of ionization of pollutant molecules [21]. The pH effect was studied by degrading 4-NP at pH 3, 5, 7 and 10 with 10 mg/L concentration of 4-NP. The degradation percentage was found to be increased with increasing pH. Maximum degradation was found at pH 5 and 7 while minimum 4-NP degradation was found at pH 3 (Fig. 3c). At pH 10 also the removal percentage was reduced slightly. Hence the Bi_2MoO_6 catalyst synthesized in this work was active for the degradation of 4-NP.

Effect of 4-NP concentration

The initial concentration of 4-NP was increased from 10 to 50 mg/L as shown in Fig. 4a. The degradation percentage was found to decrease with increasing its concentration. A maximum of 93.84 (±0.105%) degradation was achieved at 10 mg/L and the minimum degradation was found to be 78.59 (±0.389%) at 50 mg/L. However, the degradation percentage at 20 mg/L (92.26 ± 0.237%) and 30 mg/L (87.69 ± 2.107%) decreased slightly. The number of $OH^{\cdot}$ radicals generated in the degradation reaction is fixed when the catalyst and H_2O_2 concentration is fixed, and when the initial concentration of the pollutant is increased, the number of molecules to be degraded exceeds the number of $OH^{\cdot}$ radicals, so the degradation percentage decreases [60].

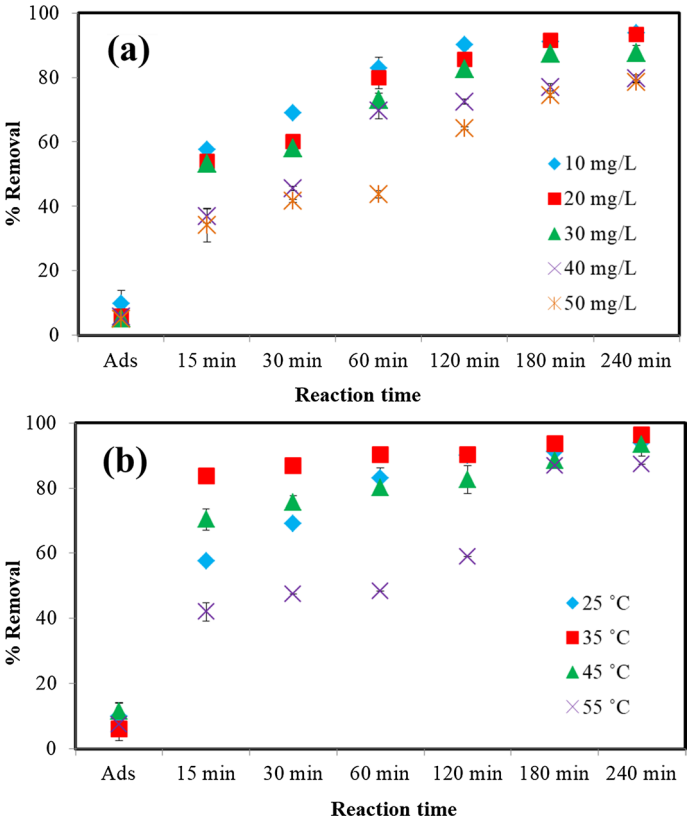

Fig. 4 **a** Effect of initial 4-NP concentration (Photocatalyst = 1 g/L, pH 7, H_2O_2 concentration = 0.05 M, Temperature = 25 °C) and **b** effect of temperature on the degradation of 4-NP (Photocatalys t = 1 g/L, pH 7, H_2O_2 concentration = 0.05 M, C_0 = 10 mg/L)

Effect of reaction time

The reaction time was studied along with the study of the initial 4-NP concentration effect. The reaction time was increased from 15 to 120 min (Fig. 4a). The degradation percentage increased with increasing reaction time. The rate of increase was higher at the initial time up to 60 min, while beyond 60 min, the rate of degradation percentage increased slowly (Fig. 4a). On an increase in reaction time, more radicals are produced, which degrade a greater number of pollutants. At the initial time, the maximum amount of H_2O_2 reacts with the vacant surface of the catalyst and produces the maximum number of $OH^{\cdot}$ radicals. Hence, the degradation rate was observed to be faster in the initial time, while after some time of reaction, the catalyst surface is covered by the adsorbed pollutant or degradation products, which reduces the generation of $OH^{\cdot}$ radicals. Furthermore, after 60 min, more than half of the pollutants and H_2O_2 reacted, leading to a decrease in their concentration in the reaction mixture due to their interaction with the catalyst, which may also cause a decrease in degradation [61].

Effect of temperature

The increase in operating temperature from 25 to 45 °C led to a slight decrease in the degradation process, and the decrease was further increased at 55 °C (Fig. 4b). The reduction in degradation percentage at higher temperatures reveals that the degradation of 4-NP by Bi_2MoO_6 was exothermic in nature and an external input of temperature adversely affected the degradation process. It might be due to the decomposition of H_2O_2 molecules at higher temperatures, which reduces the generation of $OH^{\cdot}$ radicals [62].

Degradation kinetics

The nonlinear least-squares analysis is more effective method for fitting data to kinetics in comparison to the linearized formulas. The kinetic data of 4-NP degradation was analyzed by least-square non-linear fits of pseudo-first order and pseudo-second order. The expressions for pseudo-first order and pseudo-second order kinetics are represented below in Eqs. 2 and 3 [34]:

$$C = C_0 \times \exp(-k_1 \times t) \tag{2}$$

$$\mathrm{C} = C_0/(1 + C_{0\times} k_2 t) \tag{3}$$

Here C_0 is the initial and C is the residual 4-NP concentration, and k_1 and k_2 are pseudo-first order and pseudo-second order rate constants, respectively.

Fig. 5a and b, show plots for pseudo-first order and pseudo-second order kinetics. The value of k_1 was 0.02 (± 0.003 min) and value of k_2 was 0.0044 (± 0.0001) L/mol/min. The degradation data of 4-NP was fitted best with pseudo-second

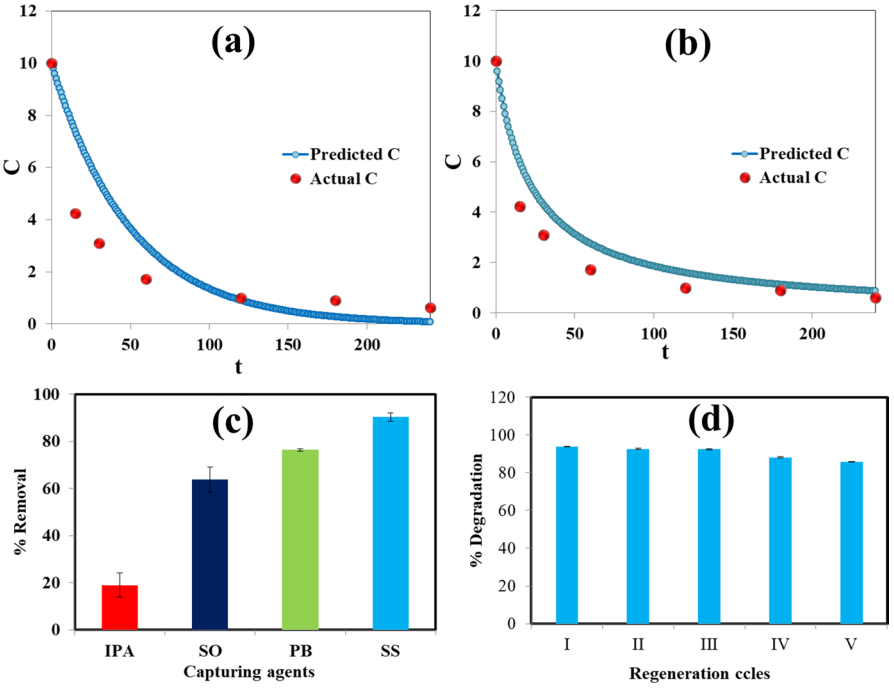

Fig. 5 **a** and **b** Plot for pseudo-first order and pseudo-second order kinetics, (Photocatalyst = 1 g/L, pH 7, C_0 = 10 mg/L, H_2O_2 concentration = 0.05 M, Temperature = 25 °C), **c** effect of different capturing agents and **d** Regeneration of catalyst

order kinetics with value of $R^2 = 0.9908$, while the value of R^2 for pseudo-first order was found to be 0.9900.

Capture of active species for the confirmation of photocatalysis

The photocatalytic process involves the generation of various active species such as hydroxyl radical ($OH^{\cdot}$), superoxide radical ($O_2^{\cdot -}$), electron hole (h^+), and free electron (e^-) by the interaction of the photocatalyst with light. These active species react with toxic organic pollutants and convert them into simpler, non-toxic forms and mineralize them ultimately. To assess the participation of these active species in the degradation process of 4-NP, different scavenging agents were added to the reaction. As a scavenging or capturing agent for $OH^{\cdot}$ isopropyl alcohol (IPA), for O_2^{-} p-benzoquinone (PBQ), for h^+ sodium oxalate (SO), and for e^- sodium sulfate (SS) was used [63, 64], and the concentration of all scavenging agents was 1 mM. Fig. 5c shows the results of the present study.

The degradation percentage was decreased most in the presence of IPA, followed by PBQ. The result indicates that the 4-NP degradation was mostly governed by the participation of $OH^{\cdot}$ radicals, which may occur due to the addition of H_2O_2 in the reaction mixture, which enhances the generation of $OH^{\cdot}$ radicals. The

Table 1 4-NP degradation efficiency of Bi_2MoO_6 in comparison with some previous reported catalysts

Catalyst	Degradation method	Removal %	References
Modified graphite felt	Electro-Fenton process	78.7% in 20 min	[65]
Hybrid montmorillonite-alginate beads	Photo-Fenton degradation	75% 40 min	[66]
Natural limonite	Electro-Fenton	96% in 6 h	[67]
$FeSO_4$	Ultrasound assisted advanced Fenton process	66.4% in 1.5 h	[22]
Iron doped TiO_2 nanoparticles	Visible light driven photocatalytic degradation	92% in 5 h	[68]
Bi_2MoO_6	Visible light driven photocatalytic degradation	93.84 ± 0.105% in 4 h	Present work

degradation of 4-NP was found to be successful via the photocatalytic degradation by the synthesized Bi_2MoO_6 catalyst. A comparison of the 4-NP degradation of Bi_2MoO_6 was compared with some previously prepared catalysts, shown in Table 1, and the efficiency of Bi_2MoO_6 was found to be better.

Regeneration of the catalyst

The regeneration ability of the catalyst is an essential factor to make its application practical. Fig. 5d shows the regeneration of the synthesized Bi_2MoO_6 catalyst, the degradation efficiency of the catalyst was very less affected by the regeneration up to five cycles. Maximum degradation was found in first cycle 93.84 ± 0.105%, while, the lowest degradation percentage was found in fifth cycle 85.62 ± 0.183. A higher degradation efficiency of the catalyst even after five regeneration cycle represents that the catalyst was stable and retained its catalytic efficiency after five cycles.

Degradation mechanism

The photocatalytic degradation of phenol by bismuth molybdate photocatalyst (P) takes place by the adsorption of light having energy more than the band gap energy of photocatalyst (2.8 eV). On the adsorption of light there is a simultaneous generation of electron and hole pair, the generated electron at conduction band is taken up by molecular oxygen to form superoxide radicals ($O_2^{\cdot -}$). Whereas, the electron holes generated on valence band react with H_2O_2 or water molecules or hydroxyl ion to form hydroxyl radicals ($OH^{\cdot}$). Both $OH^{\cdot}$ and $O_2^{\cdot -}$ are highly reactive radicals and can participate in the degradation mechanism by attacking the phenol molecules. The reactions that take place in the degradation are discussed below in Eqs. 4–7:

$$P + hv \rightarrow P\left(e_{cb}^{-}\right) + P\left(h_{vb}^{+}\right) \tag{4}$$

$$P\left(h_{vb}^{+}\right) + H_2O \rightarrow^{\circ} OH + H^{+} + P \tag{5}$$

$$P\left(e_{cb}^{-}\right) + O_2 \rightarrow O_2^{\circ -} + P \tag{6}$$

$$OH^{\cdot}/O_2^{\cdot -} + Phenol \rightarrow intermediate\ compounds \rightarrow CO_2 + H_2O \tag{7}$$

As discussed above in capture of active species the degradation of phenol was mainly driven by generation of $OH^{\cdot}$ radicals, followed by electron holes and $O_2^{\cdot -}$ radicals. The higher influence of $OH^{\cdot}$ radicals in the degradation of phenol was resulted due to addition of H_2O_2 which is good oxidizing agent and source of $OH^{\cdot}$ radicals as well. Upon catalytic decomposition one H_2O_2 molecule to two $OH^{\cdot}$ radicals take place. A proposed mechanism has been shown in Fig. 6.

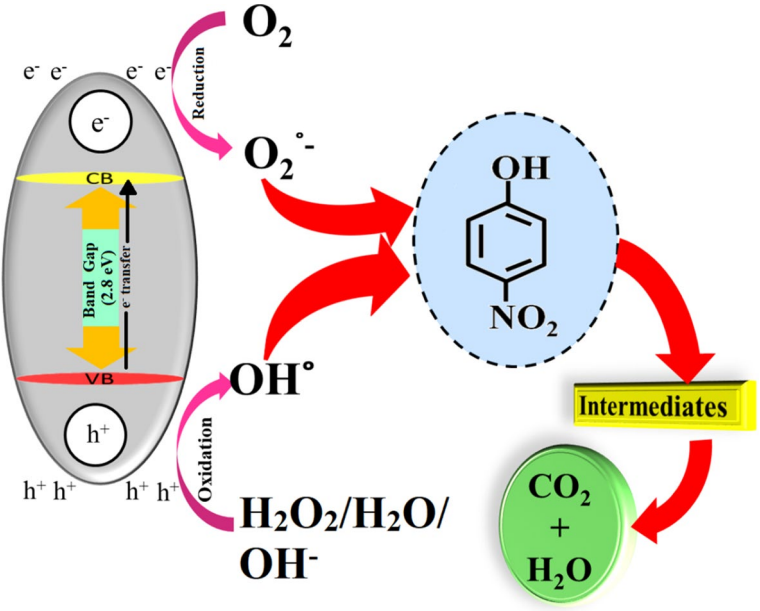

Fig. 6 Proposed mechanism for the degradation of phenol using bismuth molybdate catalyst

Conclusion

The present study concludes a successful synthesis of a visible light active photocatalyst via the continuous flow method. The catalyst synthesized was nanosized and crystalline in nature. It had good efficiencies for the degradation of 4-NP in aqueous solution. The optimum conditions for the degradation were found as catalyst concentration of 1 g/L, H_2O_2 concentration of 0.05 M, pH 5–7, initial 4-NP concentration of 10 and 20 mg/L, irradiation time of 120 min, and temperature of 25 °C. The degradation reaction was exothermic and was best followed by a pseudo-first order kinetic model. The use of various scavengers to capture active species revealed that the degradation was governed by $OH^{\cdot}$ radicals. The continuous flow synthesis method allows the mass production of nanomaterials with controllable process parameters, which saves time and overall energy input in comparison with the batch mode synthesis process. Furthermore, the degradation process carried out in this was visible light active, which ensures the use of renewable and infinite sources of light, i.e., the Sun, which further reduces the adverse environmental impacts of the remediation process and makes it affordable and scalable. In the combination of both these features, this study is a sustainable approach for the remediation of toxic water pollutants.

Acknowledgements The authors of this study gratefully acknowledge University Sophisticated Instrumentation Centre of Babasaheb Bhimrao Ambedkar University (Lucknow, India) and Sophisticated Instrumentation facility of Amity University (Noida, India) for providing facility for sample characterizations.

Author contributions BKS (Ph.D. Research Scholar) conducted experiments and did data analysis, MKG (M.Sc. Student) conducted experiments, SR (Ph.D. Research Scholar) did data curation and drafted the manuscript, HB (Assistant Professor) revised and edited the manuscript, SG (Professor) supervised the work, revised and edited the manuscript, and JS (Assistant Professor) supervised the work, revised and edited the manuscript.

Funding Non-financial.

Declarations

Conflict of interest The authors declare that they have no conflict of interests.

References

1. ATSDR (1992) Toxicological Profile for Nitro4-NPs: 2-Nitro4-NP and 4-Nitro4-NP; Public Agency for Toxic Substances and Disease Registry Health Service, Atlanta
2. Zhang C-L, Yu Y-Y, Fang Z, Naraginti S, Zhang Y, Yong Y-C (2018) Recent advances in nitroaromatic pollutants bioreduction by electroactive bacteria. Process Biochem 70:129–135. https://doi.org/10.1016/j.procbio.2018.04.019
3. Agency UEP Water quality criteria Washington DC: US Environ Prot Agency; 1976 Washington DC
4. Faghihnasiri E, Yousefi-Kebria D, Qaderi F (2018) An experimental study on the simultaneous phenol and chromium removal from water using titanium dioxide photocatalyst. Civ Eng J 4:585. https://doi.org/10.28991/cej-0309117
5. Spain J, Gibson D (1991) Pathway for biodegradation of para-nitrophenol in a Moraxella sp. Appl Environ Microbiol 57:812–819. https://doi.org/10.1128/aem.57.3.812-819.1991
6. Samuel MS, Sivaramakrishna A, Mehta A (2014) Bioremediation of p-Nitrophenol by *Pseudomonas putida* 1274 strain. J Environ Health Sci Eng 12(1):53. https://doi.org/10.1186/2052-336X-12-53
7. EPA National recommended water quality criteria table Water (2005)
8. Kulkarni M, Chaudhari A (2006) Biodegradation of p-nitrophenol by P putida. Bioresour Technol 97(8):982–988. https://doi.org/10.1016/j.biortech.2005.04.036
9. Ahmed E, Nagaoka K, Fayez M, Samir H, Watanabe G (2015) Long-term p-nitrophenol exposure can disturb liver metabolic cytochrome P450 genes together with aryl hydrocarbon receptor in Japanese quail. Jpn J Vet Res 63(3):115–127
10. Ahmed EA, Khaled HE, Elsayed AK (2021) Long-term exposure to p-Nitrophenol induces hepatotoxicity via accelerating apoptosis and glycogen accumulation in male Japanese quails. Environ Sci Pollut Res Int 28(32):44420–44431. https://doi.org/10.1007/s11356-021-13806-9
11. Agency for Toxic Substances and Disease Registry US Public Health Service (1992)
12. National Toxicology Programme (1993) (NT Toxicology and carcinogenesis studies of p-nitro4-NP (CAS No 100–02-7) in Swiss Webster Mice (Dermal Studies) US Department of Health and Human Services Public Health Service National Institute of Health
13. Arora PK, Srivastava A, Singh VP (2014) Bacterial degradation of nitrophenols and their derivatives. J Hazard Mater 266:42–59. https://doi.org/10.1016/j.jhazmat.2013.12.011
14. Rodrigues CSD, Soares OSGP, Pinho MT, Pereira MFR, Madeira LM (2017) p-Nitrophenol degradation by heterogeneous Fenton's oxidation over activated carbon-based catalysts. Appl Catal B 219:109–122. https://doi.org/10.1016/j.apcatb.2017.07.045
15. Soares OSGP, Rodrigues CSD, Madeira LM, Pereira MFR (2019) Heterogeneous Fenton-like degradation of p-nitrophenol over tailored carbon-based materials. Catalysts 9(3):258. https://doi.org/10.3390/catal9030258
16. Ji Q, Li J, Xiong Z, Lai B (2017) Enhanced reactivity of microscale Fe/Cu bimetallic particles (mFe/Cu) with persulfate (PS) for p-nitrophenol (PNP) removal in aqueous solution. Chemosphere 172:10–20. https://doi.org/10.1016/j.chemosphere.2016.12.128
17. Xiong Z, Zhang H, Zhang W, Lai B, Yao G (2019) Removal of nitrophenols and their derivatives by chemical redox: a review. Chem Eng J 359:13–31. https://doi.org/10.1016/j.cej.2018.11.111

18. Sugiyama M, Salehi Z, Tokumura M, Kawase Y (2012) Photocatalytic degradation of p-nitrophenol by zinc oxide particles. Water Sci Technol 65(10):1882–1886. https://doi.org/10.2166/wst.2012.080
19. Zhao P, Feng X, Huang D, Yang G, Astruc D (2015) Basic concepts and recent advances in nitrophenol reduction by gold- and other transition metal nanoparticles. Coord Chem Rev 287:114–136. https://doi.org/10.1016/j.ccr.2015.01.002
20. Zhang B, Li F, Wu T, Sun D, Li Y (2015) Adsorption of p-nitrophenol from aqueous solutions using nanographite oxide. Colloid Surf A Physicochem Eng 464:78–88. https://doi.org/10.1016/j.colsurfa.2014.10.020
21. Rawat S, Singh J, Koduru JR (2021) Effect of ultrasonic waves on degradation of phenol and para-nitrophenol by iron nanoparticles synthesized from Jatropha leaf extract. Environ Technol Innov 24:101857. https://doi.org/10.1016/j.eti.2021.101857
22. Pradhan AA, Gogate PR (2010) Degradation of p-nitrophenol using acoustic cavitation and Fenton chemistry. J Hazard Mater 173(1–3):517–522. https://doi.org/10.1016/j.jhazmat.2009.08.115
23. Bhatkhande DS, Pangarkar VG, Beenackers AACM (2002) Photocatalytic degradation for environmental applications–a review. J Chem Technol Biotechnol 77(1):102–116. https://doi.org/10.1002/jctb.532
24. Hoffmann MR, Martin ST, Choi W, Bahnemann DW (1995) Environmental applications of semiconductor photocatalysis. Chem Rev 95(1):69–96. https://doi.org/10.1021/cr00033a004
25. Reddy PVL, Kim KH, Kavitha B, Kumar V, Raza N, Kalagara S (2018) Photocatalytic degradation of bisphenol A in aqueous media: a review. J Environ Manag 213:189–205. https://doi.org/10.1016/j.jenvman.2018.02.059
26. Belghiti M, Tanji K, El Mersly L, Lamsayety I, Ouzaouit K, Faqir H, Benzakour I, Rafqah S (2022) Fast and non-selective photodegradation of basic yellow 28, malachite green, tetracycline, and sulfamethazine using a nanosized ZnO synthesized from zinc ore. Reac Kinet Mech Cat 135:2265–2278. https://doi.org/10.1007/s11144-022-02232-8
27. Gaidoumi EA, Loqman A, Zouheir M, Tanji K, Mertah O, Dra A, El Bali B, Kherbeche A (2021) Sol–gel fluorinated TiO_2–clay nanocomposite: study of fluor-titanium interaction on the photodegradation of phenol. Res Chem Intermed 47:5203–5228. https://doi.org/10.1007/s11164-021-04573-w
28. Ahmed S, Rasul MG, Brown R, Hashib MA (2011) Influence of parameters on the heterogeneous photocatalytic degradation of pesticides and phenolic contaminants in wastewater: a short review. J Environ Manag 92(3):311–330. https://doi.org/10.1016/j.jenvman.2010.08.028
29. Guo Q, Zhou C, Ma Z, Yang X (2019) Fundamentals of TiO_2 photocatalysis: concepts mechanisms and challenges. Adv Mater 31(50):1901997. https://doi.org/10.1002/adma.201901997
30. Kumar R, Sudhaik A, Raizada P, Hosseini-Bandegharaei A, Thakur VK, Saini A, Saini V, Singh P (2020) An overview on bismuth molybdate based photocatalytic systems: controlled morphology and enhancement strategies for photocatalytic water purification. J Environ Chem Eng 8(5):104291. https://doi.org/10.1016/j.jece.2020.104291
31. Yang G, Liang Y, Li K, Yang J, Wang K, Xu R, Xie X (2020) Engineering the dimension and crystal structure of bismuth molybdate photocatalysts via a molten salt-assisted assembly approach. J Alloys Compd 844:156231. https://doi.org/10.1016/j.jallcom.2020.156231
32. Lavakusa B, Rama Devi D, Belachew N, Basavaiah K (2020) Selective synthesis of visible light active γ-bismuth molybdate nanoparticles for efficient photocatalytic degradation of methylene blue reduction of 4-nitrophenol and antimicrobial activity. RSC Adv 10(60):36636–36643. https://doi.org/10.1039/D0RA07459D
33. Abazari R, Mahjoub AR, Shariati J, Noruzi S (2019) Photocatalytic wastewater purification under visible light irradiation using bismuth molybdate hollow microspheres with high surface area. J Clean Prod 221:582–586. https://doi.org/10.1016/j.jclepro.2019.03.008
34. Shukla BK, Gautam MK, Rawat S, Bhan C, Bhandari H, Singh J, Garg S (2022) Statistical optimization of process conditions for photocatalytic degradation of phenol with bismuth molybdate photocatalyst. Reac Kinet Mech Cat 135:2175–2194. https://doi.org/10.1007/s11144-022-02236-4
35. Gruar R, Tighe CJ, Reilly LM, Sankar G, Darr JA (2010) Tunable and rapid crystallisation of phase pure Bi_2MoO_6 (koechlinite) and $Bi_2Mo_3O_{12}$ via continuous hydrothermal synthesis. Solid State Sci 12(9):1683–1686. https://doi.org/10.1016/j.solidstatesciences.2010.07.001
36. Shukla BK, Rawat S, Bhandari H, Singh J, Garg S (2022) A sustainable approach for the synthesis of bismuth molybdate by continuous flow method using custom design reactor and their photocatalytic application for environmental remediation. Appl Nanosci 12:2497–2509. https://doi.org/10.1007/s13204-022-02524-4

37. Mishra S, Yadav SS, Rawat S, Singh J, Koduru JR (2019) Corn husk derived magnetized activated carbon for the removal of phenol and para-nitrophenol from aqueous solution: Interaction mechanism insights on adsorbent characteristics and isothermal kinetic and thermodynamic properties. J Environ Manag 246:362–373. https://doi.org/10.1016/j.jenvman.2019.06.013
38. Ren J, Wang W, Shang M, Sun S, Gao E (2011) Heterostructured bismuth molybdate composite: preparation and improved photocatalytic activity under visible-light irradiation. ACS Appl Mater Interfaces 3:2529–2533. https://doi.org/10.1021/am200393h
39. Bansal A, Kumar A, Kumar P, Bojja S, Chatterjee AK, Ray SS, Jain SL (2015) Visible light-induced surface initiated atom transfer radical polymerization of methyl methacrylate on titania/reduced graphene oxide nanocomposite. RSC Adv 5(27):21189–21196. https://doi.org/10.1039/C4RA15615C
40. Li H, Li W, Liu X, Ren C, Wang F, Miao X (2018) Fabrication of bismuth molybdate photocatalyst co-substituted by gadolinium and tungsten for bismuth and molybdenum: design and radical regulating by the synergistic effect of redox centers and oxygen vacancies for boosting photocatalytic activity. J Taiwan Inst Chem Eng 89:86–94. https://doi.org/10.1016/j.jtice.2018.04.014
41. Zheng Y, Duan F, Wu J, Liu L, Chen M, Xie Y (2009) Enhanced photocatalytic activity of bismuth molybdates with the preferentially exposed 010 surface under visible light irradiation. J Mol Catal A: Chem 303:9–14. https://doi.org/10.1016/j.molcata.2008.12.010
42. Xu J, Yue J, Niu J, Chen M (2019) Synergistic removal of Cr(VI) and dye contaminants by 0D/2D bismuth molybdate homojunction photocatalyst under visible light. Appl Surf Sci 484:1080–1088. https://doi.org/10.1016/j.apsusc.2019.04.146
43. Lavakusa B, Devi DR, Belachew N, Basavaiah K (2020) Selective synthesis of visible light active γ-bismuth molybdate nanoparticles for efficient photocatalytic degradation of methylene blue, reduction of 4-nitrophenol, and antimicrobial activity. RSC Adv 10(60):36636–36643. https://doi.org/10.1039/D0RA07459D
44. Zhang J, Ma Z (2017) Flower-like Ag2MoO4/Bi2MoO6 heterojunctions with enhanced photocatalytic activity under visible light irradiation. J Taiwan Inst Chem Eng 71:156–164. https://doi.org/10.1016/j.jtice.2016.11.030
45. Bai Y-Y, Lu Y, Liu J-K (2015) An efficient photocatalyst for degradation of various organic dyes: Ag@Ag2MoO4-AgBr composite. J Hazard Mater 307:26–35. https://doi.org/10.1016/j.jhazmat.2015.12.052
46. Cheng L, Liu L, Wang D, Yang F, Ye J (2019) Synthesis of bismuth molybdate photocatalysts for CO_2 photo-reduction. J CO2 Utilil 29:196–204. https://doi.org/10.1016/j.jcou.2018.12.013
47. Li J, Wu BZ, Zhou ZX (2018) Morphology control and optical properties of Bi_2O_3 crystals prepared by low-temperature liquid phase method. Micro Nano Lett 13(10):1443–1446. https://doi.org/10.1049/mnl.2018.5179
48. Kusuma KB, Manju M, Ravikumar CR, Dileepkumar VG, Kumar AN, Santosh MS, Murthy HCA, Gurushantha K (2022) Probe sonicated synthesis of bismuth oxide (Bi_2O_3): photocatalytic application and electrochemical sensing of ascorbic acid and lead. J Nanomater. https://doi.org/10.1155/2022/3256611
49. Reddy RKK, Kailasa S, Rani BG, Jayarambabu N, Yasuhiko H, Ramana GV, Rao KV (2019) Hydrothermal approached 1-D molybdenum oxide nanostructures for high-performance supercapacitor application. SN Appl Sci 1:1365. https://doi.org/10.1007/s42452-019-1295-5
50. Jia Q, Nguyen PK, Gu Z, Zhang X, Liu M, Tian X, Ma L, Gong L, Mu X, Chang Y (2021) N-doped bismuth molybdate decorated with Pt nanoparticles removal azo dyes efficiently via the synergistic effect of adsorption and photocatalysis. J Alloys Compd 863:158336. https://doi.org/10.1016/j.jallcom.2020.158336
51. Krishnapandi A, Muthukutty B, Chen SM, Arul KT, Shiuan HJ, Selvaganapathy M (2021) Bismuth molybdate incorporated functionalized carbon nanofiber as an electrocatalytic tool for the pinpoint detection of organic pollutant in life samples. Ecotoxicol Environ Saf 209:111828. https://doi.org/10.1016/j.ecoenv.2020.111828
52. Akpomie KG, Conradie J (2020) Biogenic and chemically synthesized *Solanum tuberosum* peel–silver nanoparticle hybrid for the ultrasonic aided adsorption of bromophenol blue dye. Sci Rep 10:17094. https://doi.org/10.1038/s41598-020-74254-y
53. Mirzaeifard Z, Shariatinia Z, Jourshabani M, Darvishi RSM (2020) ZnO photocatalyst revisited: effective photocatalytic degradation of emerging contaminants using S-doped ZnO nanoparticles under visible light radiation. Ind Eng Chem Res 59(36):15894–15911. https://doi.org/10.1021/acs.iecr.0c03192

54. Fahoul Y, Zouheir M, Tanji K, Kherbeche A (2022) Synthesis of a novel ZnAl2O4/CuS nanocomposite and its characterization for photocatalytic degradation of acid red 1 under UV illumination. J Alloys Compd 889:161708. https://doi.org/10.1016/j.jallcom.2021.161708
55. Barakat MA, Schaeffer H, Hayes G, Shah SI (2004) Photocatalytic degradation of 2-chlorophenol by Co-doped TiO_2 nanoparticles. Appl Catal B 57:23–30. https://doi.org/10.1016/j.apcatb.2004.10.001
56. Barakat MA, Tseng JM, Huang CP (2005) Hydrogen peroxideassisted photocatalytic oxidation of phenolic compounds. Appl Catal B 59:99–104. https://doi.org/10.1007/s13369-017-2632-x
57. Shukla BK, Rawat S, Gautam MK, Bhandari H, Garg S, Singh J (2022) Photocatalytic degradation of orange G dye by using bismuth molybdate: photocatalysis optimization and modeling via definitive screening designs. Molecules 27:2309. https://doi.org/10.3390/molecules27072309
58. Tony MA, Mansour SA, Tayeb AM, Purcell PJ (2018) Use of a Fenton's-like process based on nanohaematite to treat synthetic wastewater contaminated by phenol: process investigation and statistical optimization. Arab J Sci Eng 43:2227–2235. https://doi.org/10.1007/s10653-017-9946-1
59. Zhang J-H, Zou H-Y, Ning X-A, Lin M-Q, Chen C-M, An T-C, Sun J (2018) Combined ultrasound with Fenton's treatment for the degradation of carcinogenic polycyclic aromatic hydrocarbons in textile dying sludge. Environ Geochem Health 40:1867–1876. https://doi.org/10.1007/s10653-017-9946-1
60. Ahsan MA, Santiago ARP, Rodriguez A, Maturano-Rojas V, Alvarado-Tenorio B, Bernal R, Noveron JC (2020) Biomass-derived ultrathin carbon-shell coated iron nanoparticles as high-performance tri-functional HER ORR and Fenton-like catalysts. J Clean Prod 275:124141. https://doi.org/10.1016/j.jclepro.2020.124141
61. Rawat S, Singh J (2022) Fenton like oxidative degradation of toxic water pollutants by iron nanoparticles synthesized via facile green route using waste iron rust as the iron precursor. Environ Eng Res. https://doi.org/10.4491/eer.2021.621
62. Mokrema M, Sung LD (2020) Photocatalytic degradation of methylene blue with P25/graphene/polyacrylamide hydrogels: optimization using response surface methodology. J Hazard Mater 400:123314. https://doi.org/10.1016/j.jhazmat.2020.123314
63. Shu YJ, Yan SR, Dong KJ, Chen JW (2018) Preparation of novel mesoporous photocatalyst Bi_4O_5Br 2/SBA-15 with enhanced visible-light catalytic activity. Open J Appl Sci 8:532–544. https://doi.org/10.4236/ojapps.2018.811043
64. Susanti YD, Afifah N, Saleh R (2017) Multifunctional photocatalytic degradation of methylene blue using $LaMnO_3/Fe_3O_4$ nanocomposite on different types of graphene. J Phys Conf Ser 820(1):012021. https://doi.org/10.1088/1742-6596/820/1/012021
65. Zhou L, Zhou M, Zhang C, Jiang Y, Bi Z, Yang J (2013) Electro-Fenton degradation of p-nitrophenol using the anodized graphite felts. Chem Eng J 233:185–192. https://doi.org/10.1016/j.cej.2013.08.044
66. Barreca S, Colmenares JJV, Pace A, Orecchio S, Pulgarin C (2014) Neutral solar photo-Fenton degradation of 4-nitrophenol on iron-enriched hybrid montmorillonite-alginate beads (Fe-MABs). J Photochem Photobiol A 282:33–40. https://doi.org/10.1016/j.jphotochem.2014.02.008
67. Tao HC, Wei XY, Zhang LJ, Lei T, Xu N (2013) Degradation of p-nitrophenol in a BES-Fenton system based on limonite. J Hazard Mater 254:236–241. https://doi.org/10.1016/j.jhazmat.2013.03.061
68. Sood S, Umar A, Mehta SK, Kansal SK (2015) Highly effective Fe-doped TiO_2 nanoparticles photocatalysts for visible-light driven photocatalytic degradation of toxic organic compounds. J Colloid Interface Sci 450:213–223. https://doi.org/10.1016/j.jcis.2015.03.018

Authors and Affiliations

Brijesh Kumar Shukla[1] · Mayank Kumar Gautam[2] · Shalu Rawat[2] · Hema Bhandari[3] · Jiwan Singh[2] · Seema Garg[1]

[1] Department of Chemistry, Amity Institute of Applied Sciences, Amity University, Sector-125, Noida, Uttar Pradesh 201313, India

[2] Department of Environmental Science, Babasaheb Bhimrao Ambedkar University, Lucknow 226025, India

[3] Department of Chemistry, Maitreyi College, University of Delhi, New Delhi 110021, India